www.czasopisma.pan.pl PAN www.journals.pan.pl
jet INTL JOURNAL OF ELECTRONICS AND TELECOMMUNICATIONS, 2011, VOL. 57, NO. 1, PP. 97–102
Manuscript received January 19, 2011; revised February 2011. DOI: 10.2478/v10177-011-0014-y

A Short Range Synthetic Aperture Imaging Radar with Rotating Antenna

Faiza Ali, Alexander Urban, and Martin Vossiek

***Abstract*—The design of a short range synthetic aperture imaging radar is introduced in this paper. A radar hologram is acquired using a small omnidirectional antenna that is mounted on a rotating platform. After each turn of the platform a high resolution 360° 2D image is reconstructed; a rotating window function optimizes the reconstructed image function to get the best image focus for detecting both weak and strong scatterers. The rotating window function depends on the target direction and is executed for each image point and each target direction. The size of the synthetic aperture – and thus the lateral resolution of the imaging system – is determined by the diameter of the circular antenna trajectory. In contrast to common radar scanner concepts that utilize highly directional and thus bulky antennas, the proposed scanner concept has the advantage of using a small, lightweight omni-directional antenna. The developed radar system is much more compact and the scanning mechanics are significantly simplified. Furthermore, an omni-directional antenna offers very straightforward options for powering the radar on the rotation platform. Measurement results obtained with a 24 GHz FMCW short range radar sensor illustrate the performance of the proposed SAR imaging method.**

***Keywords*—Radar, synthetic aperture, scanning, imaging.**

I. Introduction

RADAR scanners have been used for imaging and detection purposes in aviation, navigation, space and military applications [1], [2]. Increasingly nowadays radar imaging is used in commercial applications in the areas of robotics, automation, security and vehicular systems [3], [4]. The focus in these new application areas is on detecting all objects in an environment, including weak scatterers that are possibly masked by strong targets.

With the growing use of radar imaging in many application areas, a myriad of signal processing algorithms have been developed to optimize detection methods and to improve the image resolution [5], [6]. The classical scanning radar system utilizes a direct imaging technique with a rotating directional antenna or an array of antennas. The lateral resolution of direct imaging methods is a function of the antenna beam angle, and is defined as:

$$\delta_{lat} \sim z_0 \cdot \lambda / D, \tag{1}$$

where z_0 is the distance from the radar unit to the target scene, λ is the radar signal wavelength and D is the antenna or array size. Large antennas are needed to achieve good lateral resolution. The equipment needed is therefore big and cumbersome.

F. Ali, A. Urban, and M. Vossiek are with the Clausthal University of Technology, Institute of Electrical Information Technology, Leibnizstr. 28, D-38678 Clausthal-Zellerfeld, Germany (e-mails: {ali, urban, vossiek}@iei.tu-clausthal.de).

It is well known that a synthetic aperture radar approach delivers images with high lateral resolution. In this case, small omni-directional antennas generate a hologram from which the final image is reconstructed.

In radar imaging weak scatterers can be masked by strong targets if both targets are sufficiently near each other. This raises detection issues in radar imaging. The lateral resolution of an SAR system can also be expressed as "(1)," with D denoting the size of a synthetic aperture generated by the antenna movement. Klausing [7] shows that a high resolution 360° 2D image can be produced by synthetic aperture radar with rotating antennas (ROSAR).

The commercial application of SAR has been dogged in the past by the prohibitive computational effort required by the reconstruction algorithms. Advances in embedded systems have meant that SAR is now a more practical and attractive alternative.

In this paper we present an imaging approach based on a high resolution synthetic aperture 360° 2-D imaging radar scanner. The system is based on a FMCW radar unit and a small omni-directional antenna mounted on a small rotating platform.

II. Scanner Concept

A. System Setup and Signal Specifications

The proposed SAR scanner setup is depicted in Fig. 1. A rotating radar platform with a radius r_{sc} is located at the origin ($x = 0$, $y = 0$) of a coordinate system. The radar sensor comprises an omni-directional transmit and receive antenna that is located at the edge of the circular platform at position $\boldsymbol{a}_n = (x_n, y_n, z_0)^T$. A point on a reflecting target in the target scene is denoted by $\boldsymbol{p}_r = (x_r, y_r, z_0)^T$.

B. Signal Transmission Model

In order to clarify the system, a block diagram of the radar signal transmission model is shown in Fig. 2.

As illustrated in Fig. 1 the radar antenna located at position $\boldsymbol{a}_n = (x_n, y_n, z_0)^T$ transmits a signal $s_{tx}(t)$. The radar signal travels to the target at position $\boldsymbol{p}_r = (x_r, y_r, z_0)^T$ and is reflected back to the radar unit. The distance between the radar unit and the target can be calculated by:

$$d_n = |\boldsymbol{p}_r - \boldsymbol{a}_n| = \sqrt{(x_r - x_n)^2 + (y_r - y_n)^2 + z^2}. \tag{2}$$

The signal received by the radar unit is determined by the spatial and temporal transfer function of the complete transmission path. The function $\tau(t)$ denotes the round trip time of flight (RTOF) of the radar signal depending on the

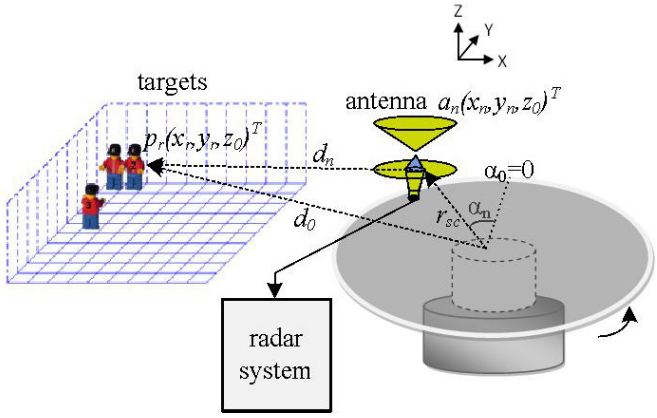

Fig. 1. Radar scanner and test setup.

distance between the radar unit and the target, and the relative velocity of the object with respect to the radar unit.

If we assume the object is stationary, the temporal change of the distance is determined by the angular velocity of the rotating antenna [5]. Hence we get:

$$\tau(t) = \frac{2 \cdot d_n(t)}{c}, \text{with}$$
$$d_n(t) = d_0 - r_{sc} \cdot \cos(\omega_{sc} \cdot t + \alpha_0), \quad (3)$$

where ω_{sc} is the angular velocity of the rotating platform and α_0 is its angle at $t = 0$. For the sake of simplicity we assume that α_0 is 0 at $t = 0$.

The FMCW radar beat signal is obtained by mixing the received signal with the transmit signal. After lowpass-filtering, the FMCW radar beat signal is given by [8]:

$$s_b(t) = A_b \cdot e^{j \cdot (\omega_c \cdot \tau(t) + \mu \cdot \tau(t) \cdot t)}, \quad (4)$$

where A_b is the signal amplitude, ω_c is the radian frequency of the RF carrier and μ is the sweep rate. The sweep rate is defined as the quotient of the radar signal sweep bandwidth B and the sweep duration T. By inserting (3) into (4) we can derive the beat signal as:

$$s_b(t) = A_b \cdot e^{\frac{j \cdot 2}{c} \cdot [\omega_c \cdot (d_0 - r_{sc} \cdot \cos(\omega_{sc} \cdot t)) + \mu \cdot (d_0 - r_{sc} \cdot \cos(\omega_{sc} \cdot t)) \cdot t]}. \quad (5)$$

The instantaneous frequency $\omega_b(t)$ of this signal can be calculated as:

$$\omega_b(t) = \frac{d \arg\{s_b(t)\}}{dt}$$
$$= \mu \cdot \frac{2d_0}{c} - \frac{2 \cdot v_{sc}}{c \cdot \omega_{sc}} \cdot \cos(\omega_{sc} \cdot t) + \frac{2\omega_c \cdot v_{sc}}{c} \cdot \sin(\omega_{sc} \cdot t) \quad (6)$$
$$+ \mu \cdot \frac{2 \cdot v_{sc}}{c} \cdot \sin(\omega_{sc} \cdot t) \cdot t]$$

Since the velocity v_{sc} of the radar unit

$$v_{sc} = r_{sc} \omega_{sc}, \quad (7)$$

is much smaller than the speed of light, we can ignore the last term in (6). Finally, by substituting v_{xsc}, v_{xsc} as the horizontal and vertical components of the scanner velocity, we obtain:

$$\omega_b(t) = \omega_b = \mu \cdot \frac{2d_0}{c} - \frac{2 \cdot v_{xsc}}{c \cdot \omega_{sc}} + \frac{2\omega_c \cdot v_{ysc}}{c}. \quad (8)$$

The Fourier transform of (5) that leads to the FMCW radar echo profile $e(d, v_{sc})$ can be derived by considering (8) and the Fourier modulation theorem. We also introduce a window function $w(t)$ since the beat signal is only defined during the time interval T. With $W(d)$ as the Fourier transform of $w(t)$ the final FMCW radar echo profile $e(d, v_{sc})$ is given by:

$$e(d, v_{sc}) = A_b' |W(d - d_n)| e^{j \frac{2 \cdot \omega_c \cdot d_n}{c}}. \quad (9)$$

III. Reconstruction Algorithm

The broadband holographic reconstruction algorithm is based on optimal spatial and temporal filtering [9], [10]. To calculate the target position $\boldsymbol{p}_r = (x_r, y_r, z_0)^T$ in the 2D plane, the echo profile $E(\omega_d)$ of the received signal $e(d_n)$ at each radar sensor's position $\boldsymbol{a}_n = (x_n, y_n, z_0)^T$ is correlated with the hypothetical echo profile function $F(\omega_d, d_r, a_n)$ as:

$$b_r(x, y, z) = \left| \sum_{n=1}^{N} \int_{\omega_d} E(\omega_d) \cdot F^{-1}(\omega_d, a_n, p_r) \cdot d \cdot d\omega_d \right|, \quad (10)$$

where ω_d is the beat frequency related to distance d_n. The correlation function $F^{-1}(\omega_d, d_n, a_n)$ used, is an inverse filter, which can be calculated based on the inverse of the Fourier transform of (9), If we assume an AWGN channel model it is defined as:

$$F^{-1}(\omega_d, d_n, a_n) = \frac{1}{\alpha} \cdot e^{j\omega_d \cdot d_n} \cdot e^{-j \frac{2\omega_c}{c} \cdot d_n}. \quad (11)$$

The attenuation factor α is normally a function of d_n. In a simple AWGN channel model it can be approximated by $\alpha = 1/d_n^2$ [9] to yield:

$$b_r(x, y, z) = \left| \sum_{n=1}^{N} d_n^2 \cdot e^{-j \frac{2\omega_c}{c} d_n} \cdot \int E(\omega_d) \cdot e^{j\omega_d \cdot d_n} d\omega_d \right|. \quad (12)$$

The integral over the circular frequency corresponds to an inverse Fourier transform and thus provides the signal received at $t = \tau_n$. The final reconstruction provision is:

$$b_r(x, y, z) = \left| \sum_{n=1}^{N} d_n^2 \cdot e(d = d_n) \cdot e^{-j \frac{2\omega_c}{c} d_n} \right|. \quad (13)$$

If there is a target at position $\boldsymbol{p}_r$ then an echo profile occurs in the signal received at each point in space at $t = \tau_n$. The correct summation of echo profiles with respect to the time of flight coherently superimposes the reflected contributions and gives rise to a high value at $\boldsymbol{b}_r = (x, y, z)$. If there is no target at position $\boldsymbol{p}_r$ the reflections are superimposed incoherently and thus lead to a significantly weaker image signal.

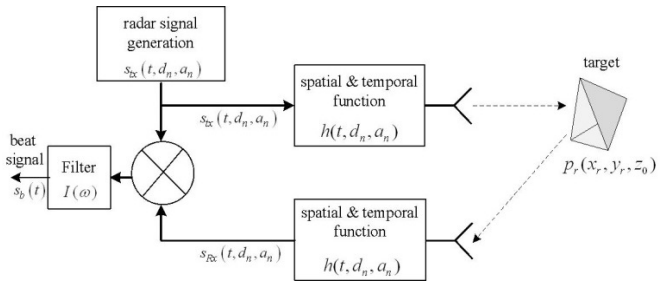

Fig. 2. Signal transmission model.

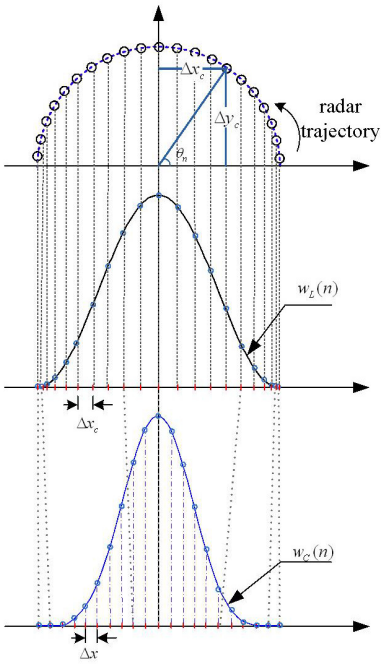

Fig. 3. Redistribution of the window functions for a circular radar trajectory.

IV. Image Optimization

It is well known that the side-lobe level of an antenna array, and the side-lobe level of the point-spread function of an SAR system, can be reduced by using a suitable weighting function [5], [6]. In our system we apply a hamming-like window function $w_c(n)$ that is adapted to the circular aperture as follows:

$$b_r(x,y,z) = \left| \sum_{n=1}^{N} w_c(n) \cdot d_n^2 \cdot e(d=d_n) \cdot e^{-j\frac{2\omega_c}{c}d_n} \right|. \quad (14)$$

Given a linear SAR trajectory with length L and N equally spaced measurement points, the hamming window function $w_L(n) = w_L(l(n))$ is expressed as:

$$w_L(l(n)) = \begin{cases} 0.54 - 0.46 \cdot \cos(2\pi \cdot l(n)/L) & 0 \le n \le N \\ 0 & \text{otherwise} \end{cases} \quad (15)$$

with: $l(n) = n \cdot \Delta x$,
where Δx is the spacing between the measurement points.

In the case of a circular trajectory, the function $l(n)$ in (15) must be adjusted in accordance with the projection of the circular trajectory to a linear trajectory perpendicular to the actual imaging direction. This gives rise to a new window function $w_c(n)$. For this window function the function $l_c(n)$ is defined as:

$$l_c(n) = n \cdot \Delta x_c = n \cdot r_{sc} \cdot \cos\theta_n \quad (16)$$

where θ_n is the radar trajectory rotation angle and $\Delta x_c = r_{sc} \cdot \cos\theta_n$, $\Delta y_c = r_{sc} \cdot \sin\theta_n$ denote the spacing between the measurement points in x and y direction.

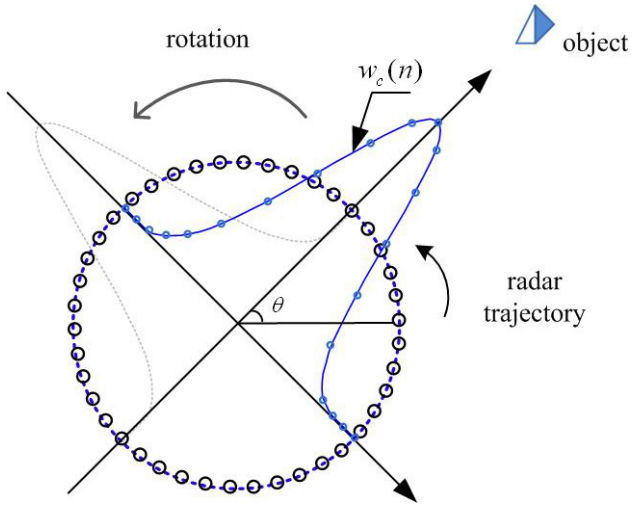

Fig. 4. Direction-dependent window function.

Hence we get the hamming-like window function as:

$$w_c(n) = \begin{cases} 0.54 - 0.46 \cdot \cos(2\pi \cdot l_c(n)/L) & 0 \le n \le N \\ 0 & \text{otherwise} \end{cases} \quad (17)$$

The application of the hamming-like window function $w_c(n)$ for each reconstructed image point depends on the target direction, that is, a different window weight is attributed to each image point in each target direction.

We use the point spread function (PSF) as an imaging quality metric. The lateral and axial resolution of the target in Fig. 5 are calculated at the -6dB limits of the PSF. Note that the use of the rotating window function minimizes the side lobe level for each target in the reconstructed image function at the cost of a slightly reduced resolution. The lateral resolution δ_{lat} given by (1) for $z_0 = 1.5$ m and $D = 2r_{sc}$ matches the actual lateral resolution of $\Delta_{lat} \approx 15$cm. The axial resolution $\delta_{ax} = c/B$ depends on the sweep bandwidth.

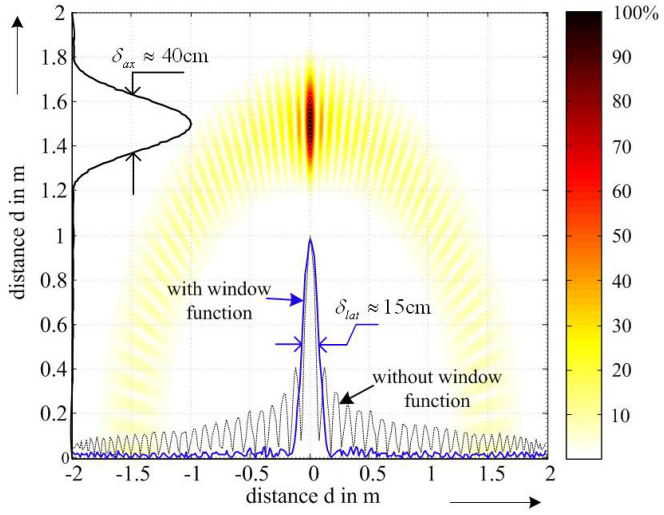

Fig. 5. 2D image of a simulated target. Projection of the image function to the lateral axis with/without applied window function. As visible the lateral and axial resolution are 15 [cm] and 40 [cm].

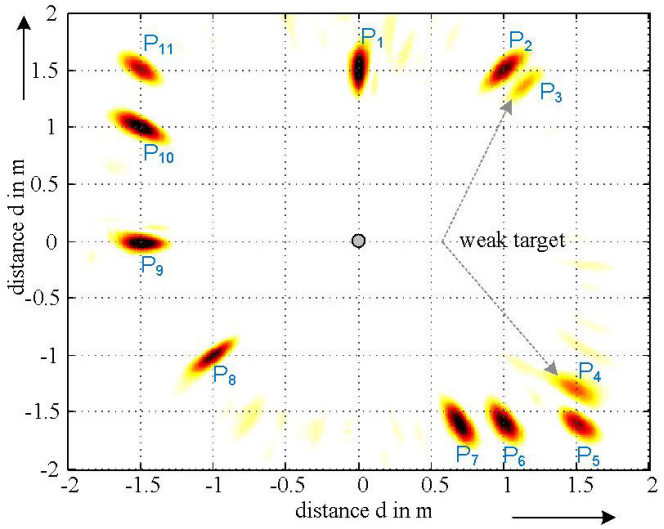

Fig. 6. 2D image of 9 strong and 2 weak simulated targets using the hamming-like window function.

The calculated axial resolution is approximately 40 cm for the given parameters – this is also confirmed by the test results.

Fig. 6 shows a simulated 2D image of a scenario with 9 strong and 2 weak simulated targets in the coordinate system (x, y, z) located at p_1=(0,1.5,0) m, p_2=(1,1.5,0) m, p_3=(1.15,1.38,0) m p_4=(1.5,-1.3,0) m, p_5=(1.5,-1.6,0) m, p_6=(1,-1.6,0) m, p_7=(0.7,-1.6,0) m, p_8=(-1,-1,0) m, p_9=(-1.5,0,0) m, p_{10}=(-1.5,1,0) and p_{11} =(-1.5,1.5,0) m with a radar center frequency of 24.5 GHz, sweep bandwidth $B = 800$ MHz (wideband mode), sweep duration $T = 5$ ms and aperture radius $r_{sc} = 6.3$ cm. Using the method presented in [11], the weak scatterers would be masked by the side lobes of the strong targets in their vicinity. Applying the rotating hamming-like window function minimizes the side lobes for optimal separation of weak and strong targets.

V. System Setup

A. Antenna Design

There is no need for an antenna with small beam width in synthetic aperture radar – thus, the physical size can be small. The size of the synthetic aperture and the lateral resolution δ_{lat} are defined by the radar trajectory D. Referring to [11],

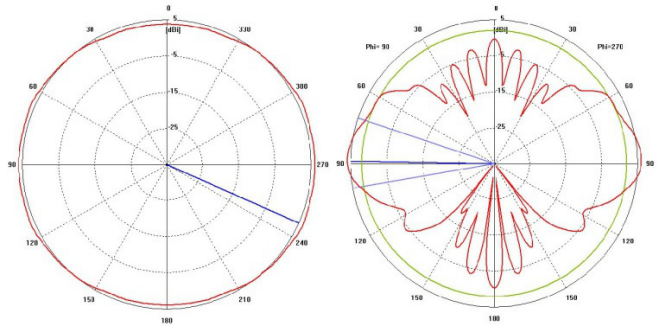

Fig. 7. Horizontal and vertical radiation pattern of the omni-directional antenna (main lobe magnitude=6 [dBi], side lobe level=-3.9 [dBi]).

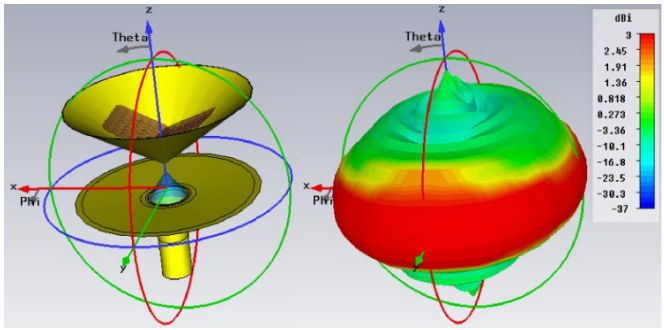

Fig. 8. Design and far-field radiation pattern of the omni-directional antenna with polyethylene insert.

we deployed an omni-directional reflector antenna as proposed in [12], [13]. The reflector radii of this 24.5-GHz antenna are $r_1 = 5$ cm, $r_2 = 2r_1$, $r_3 = r_4 = 2.5 \cdot \lambda$.

A small horn antenna is used as radiation source. The reflectors are made of thin copper metal sheet, which results in a lightweight antenna.

Dielectric rod antennas are good candidates for feed antennas due to their low polarization cross-coupling and their potential for very dense packing [14], [15]. To focus the radiation source we inserted a specially shaped piece of dielectric high density polyethylene (HDPE, $\epsilon_r = 2.32 \ldots 2.34$, $\delta_\epsilon = 21. \ldots 9.1 \times 10^4$) in the radiation path inside the small horn antenna. Since surface waves radiate at surface discontinuities, they run along the dielectric polyethylene surface as guided waves and only radiate at the tip of the dielectric taper. This enabled us to get a very small antenna beam width and to downsize the reflectors of the omni-directional antenna. The antenna design and its horizontal and vertical radiation pattern with the reflector radii $r_1 = 3$ cm are illustrated in Fig.7 and Fig.8, and Fig. 9 shows a view of the antenna design.

Another advantage of the scanning antenna with an omni-directional pattern is that no slip ring is needed to connect the antenna on the rotating platform with the system base: if the antenna itself is pivot-mounted, a simple flexible cable is all that is needed.

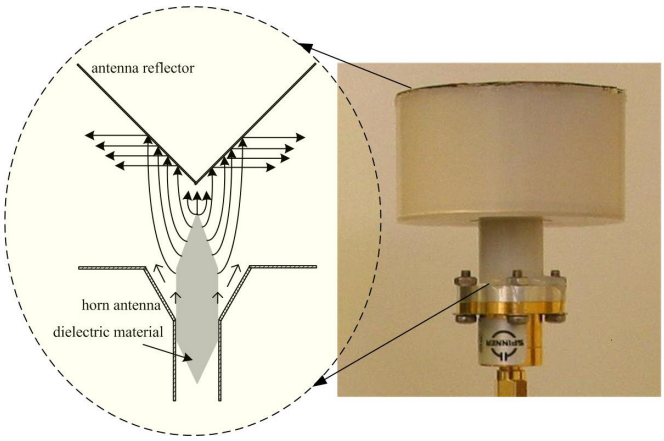

Fig. 9. Design and photo of omni-directional antenna with dielectric taper.

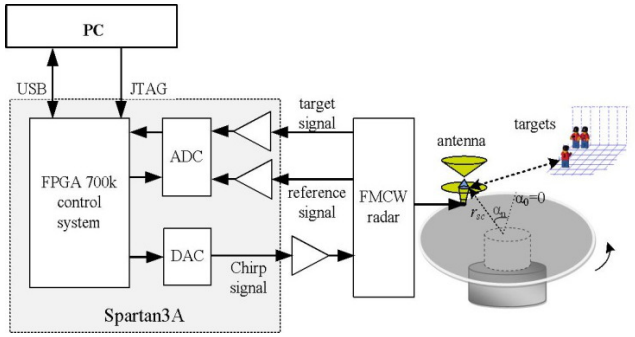

Fig. 10. Block diagram of proposed radar system.

B. Radar Sensors and FPGA

We implemented the signal evaluation algorithms on a field programmable gate array (FPGA) to achieve real time processing. We used VHDL (Very High Speed Integrated Circuit Hardware Description Language) to implement parallel signal processing and to control all peripheral units such as ADC, DAC, radar, USB etc.

A Siemens / Milltronics 24GHz FMCW radar system served as the radar frontend [16]. The complete radar system setup is depicted in Fig. 10. The VCO control signal is generated by a 16-bit digital-to-analog converter. The radar signals are amplified, filtered and sampled with a 14-bit, 1.5 MS/s analog-to-digital converter. The beat signal phase error is corrected in the FPGA by means of the constant phase interval sampling technique presented in [16]. The phase-error-free beat signal is transferred via USB to a PC where the image is reconstructed using the echo profiles.

VI. Test Results

We describe here the actual results we obtained using a FMCW radar system with a center frequency of $f_m = 24.72$ GHz, a sweep bandwidth of $B = 800$ MHz, a sweep duration of $T = 5$ ms and a measurement rate of 200 Hz.

Fig. 11 shows a room (15.12×7.85 m), filled with various objects that were scanned by the radar system. The walls of the room labeled 1 appear at range (7.98 m, 6.99 m, 3.1 m and 4.75 m). The other objects consist of: a corner reflector with RCS ($\sigma = 10.4 \times 10^{-5}$ m^2, $r_2 = 5.19$ m) labeled 2; a reflection plate (50×50 cm, $r_4 = 3.89$ m) labeled 4; two metal columns labeled 3 and 5 with $r_3 = 2.1$ m, $r_5 = 3.5$ m; a switching cabin (3×2 m) labeled 6 with $r_6 = 4.8$ m and a window front labeled 7 with $r_7 = 3.43$ m. We obtained a high-resolution radar image of the scene. Objects with flat surfaces are typically difficult to detect with stationary scanning systems due to mirror-like reflections. Only if the emitted radiation hits the flat surface at right angles, the reflected radiation can be picked up by the radar system. In contrast, we obtained very good images of multi-directional scattering objects.

Referring to the measurement result in [11], we can see that the side-lobe level has been reduced to get a good focus and good target detection. Fig. 12 shows that the strong target like a corner reflector (labeled 2) is already separated from another target like wall (labeled 1).

The distance between two aperture points should not extend beyond $\lambda/2$ to meet the spatial sampling theorem criteria [17]. Taking the wavelength of the radar system into account a minimum of 65 measurements per rotation are needed to comply with the spatial sampling theorem. The system scan rate is 3 scans per second given a 200-Hz measuring rate. The sampling rate is currently limited by the PC reconstruction and visualization software. These speed limitation issues can be eliminated by running all signal processing algorithms in the FPGA.

References

[1] G. M. Kirkpatrick, "Development of a Monopulse Radar System," *IEEE Transactions on Aerospace and Electronic Systems*, vol. 45, pp. 807–818, April 2009.

[2] D. Vivet, P. Checchin, and R. Chapuis, "On the Fly Localization and Mapping Using a 360° Field-of-View Microwave Radar Sensor," in *IEEE International Conference on Intelligent Robots Systems*, St Louis, MO, USA, October 2009, pp. 23–28.

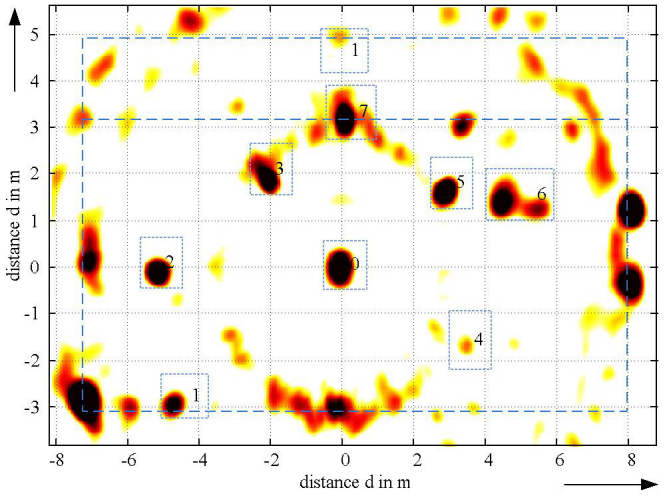

Fig. 11. 2D imaging results from a test run in a room (15.12 [m]×7.85 [m]) with a variety of objects at different locations around the room.

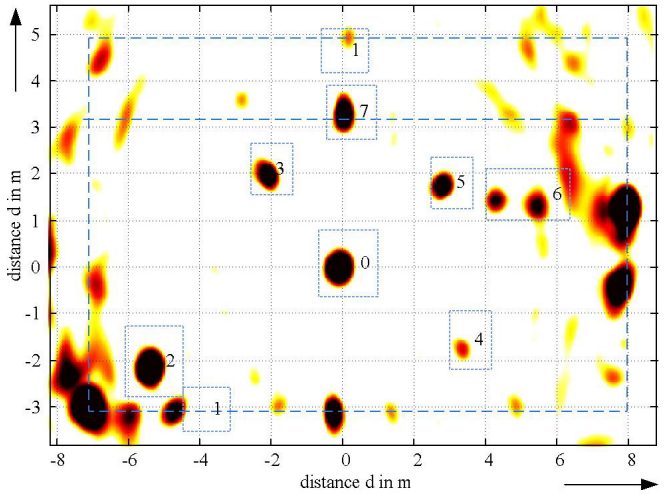

Fig. 12. 2D imaging results from a test run in a room (15.12 [m]×7.85 [m]) with an object near the wall.

[3] S. K. Boehmke, J. Bares, E. Mutschler, and N. K. Lay, "A High Speed 3D Radar Scanner for Automation," *IEEE International Conference on Robotics and Automation Proceedings*, vol. 4, pp. 2777–2782, 1998.
[4] P. Checchin, F. Gérossier, C. Blanc, R. Chapuis, and L. Trassoudaine, "Radar Scan Matching SLAM Using the Fourier-Mellin Transform," in *IEEE Int. Conf. on Field and Service Robotics (FSR)*, Cambridge, Massachusetts, USA, July 2009.
[5] S. Nordebo, Z. Zang, and I. Claesson, "A Semi-Infinite Quadratic Programming Algorithm with Applications to Array Pattern Synthesis," *IEEE Transactions on Circuit and Systems*, vol. 48, no. 3, pp. 225–232, March 2001.
[6] S. Wu and J. Zhang, "Research of Array Geometry for Smart Antenna," in *6th International Symposium on Antennas, Propagation and EM Theory*, China, 2003, pp. 294–298.
[7] H. Klausing, "Feasibility of a Synthetic Aperture Radar with Rotating Antennas (ROSAR)," in *Microwave 19th European Conference*, September 1989, pp. 287–299.
[8] F. Ali and M. Vossiek, "Detection of Weak Moving Targets Based on 2-D Range-Doppler FMCW Radar Fourier Processing," in *Proceedings of 5th German Microwave Conference*, March 2010, pp. 214–217.
[9] M. Vossiek, A. Urban, S. Max, and P. Gulden, "Inverse Synthetic Aperture Secondary Radar Concept for Precise Wireless Positioning," *IEEE Transactions on Microwave Theory and Techniques*, vol. 55, pp. 2447–2453, 2007.
[10] M. Vossiek, R. Roskosch, and P. Heide, "Precise 3-D Object Position Tracking Using FMCW Radar," in *Proceedings of 29th European Microwave Conference*, vol. 1, October 1999, pp. 234–237.
[11] F. Ali, A. Urban, and M. Vossiek, "A High Resolution 2D Omnidirectional Synthetic Aperture Radar Scanner at K Band," in *2010 European Radar Conference (EuRAD)*, Paris, France, September 2010, pp. 503–506.
[12] A. Nosich, R. Sauleau, and Y. V. Gandel, "Classical ADE and PACO Omni-directional Dual Reflector Antennas Simulated in 2-D Using a Nystrom-Type MDS Algorithm," in *Proceedings of 39th European Microwave Conference*, 29 September-1 October 2009, pp. 858–861.
[13] W. Menzel and R. Leberer, "Folded Reflect Array Antennas for Shaped Beam Applications," in *First European Conference on Antennas and Propagation*, Nice, France, 6-10 November 2006, pp. 1–4.
[14] J. Richter and L.-P. Schmidt, "Dielectric Rod Antennas as Optimized Feed Elements for Focal Plane Arrays," in *Antennas and Propagation Society International Symposium*, 2005, pp. 667–670.
[15] J. Richter, M. Müller, and L.-P. Schmidt, "Measurement of Phase Centers of Rectangular Dielectric Rod Antennas," in *Antennas and Propagation Society International Symposium*, 2004, pp. 743–746.
[16] M. Vossiek, P. Heide, M. Nalezinski, and V. Magori, "Novel FMCW Radar System Concept with Adaptive Compensation of Phase Errors," in *Proceedings of 26th European Microwave Conference*, Prague, Czech Republic, 1996, pp. 135–139.
[17] M. I. Skolnik, *Radar Handbook*, 2nd ed. New York: McGraw-Hill Professional, 1990.